Hole-Spin Driving by Strain-Induced Spin-Orbit Interactions

José Carlos Abadillo-Uriel, Esteban A. Rodríguez-Mena, Biel Martinez, and Yann-Michel Niquet*
Université Grenoble Alpes, CEA, IRIG-MEM-L_Sim, 38000 Grenoble, France

(Received 7 December 2022; accepted 16 July 2023; published 1 September 2023)

Hole spins in semiconductor quantum dots can be efficiently manipulated with radio-frequency electric fields owing to the strong spin-orbit interactions in the valence bands. Here we show that the motion of the dot in inhomogeneous strain fields gives rise to linear Rashba spin-orbit interactions (with spatially dependent spin-orbit lengths) and g-factor modulations that allow for fast Rabi oscillations. Such inhomogeneous strains build up spontaneously in the devices due to process and cool down stress. We discuss spin qubits in Ge/GeSi heterostructures as an illustration. We highlight that Rabi frequencies can be enhanced by 1 order of magnitude by shear strain gradients as small as 3×10^{-6} nm^{-1} within the dots. This underlines that spins in solids can be very sensitive to strains and opens the way for strain engineering in hole spin devices for quantum information and spintronics.

DOI: 10.1103/PhysRevLett.131.097002

Hole spins in semiconductor quantum dots [1] show versatile interactions with electric fields owing to the strong spin-orbit interaction (SOI) in the valence bands [2–4]. This allows for fast electrical manipulation of hole spin qubits [5–11] and for strong spin-photon interactions [12–15] suitable for long-range entanglement. The SOI, however, couples the spin to electrical and charge noise; yet recent works have shown how dephasing "sweet spots" can be engineered to limit decoherence [15–18]. Ge/GeSi heterostructures have, in particular, made outstanding progress in the past two years [11,19,20], with the demonstration of a four qubits processor [21] and of charge control in a sixteen dots array [22].

The manipulation of hole spins by resonant ac electric fields involves a variety of physical manifestations of SOI. Rashba and Dresselhaus interactions couple the spin to the momentum of the hole, and give rise to an effective time-dependent magnetic field when the dot is shaken as a whole by the ac electric field [23,24]. The modulations of the gyromagnetic g factors of the hole resulting from the deformations of the moving dot may also drive spin rotations (g-tensor modulation resonance or g-TMR) [6,25–27]. The physics of SOI has been extensively investigated in Ge/GeSi heterostructures [28–33]; the role of the nonseparability of the confinement potential and of the inhomogeneity of the ac electric field has in particular been highlighted [34]. Yet the above mechanisms hardly seem sufficient to explain the large Rabi frequencies reported in some experiments [11,20,21].

In this Letter, we show that inhomogeneous strains give rise to specific linear Rashba and g-TMR mechanisms allowing for efficient electrical hole spin manipulation. We take Ge/GeSi heterostructures as an illustration, and demonstrate a tenfold increase in the Rabi frequencies for shear strain gradients as small as 3×10^{-6} nm^{-1}, arising naturally from differential thermal contraction between materials [35]. These mechanisms are likely ubiquitous in hole spin devices, but their fingerprints can easily be mingled with those of conventional (purely kinetic) Rashba SOI and g-TMR. This emphasizes how much spins in solids can be sensitive to strains [27,36–38].

Theory.—We consider a hole moving in a potential $V(\mathbf{r})$ and a homogeneous magnetic field $\mathbf{B}$. The heavy-hole (HH) and light-hole (LH) Bloch functions can be mapped, respectively, onto the $J_z = \pm\frac{3}{2}$ and $J_z = \pm\frac{1}{2}$ components of a $J = \frac{3}{2}$ spin. The envelopes of these four Bloch functions fulfill a set of differential equations defined by the Luttinger-Kohn Hamiltonian [39,40]:

$$H = H_{\mathrm{K}} + H_{\varepsilon} + H_{\mathrm{Z}} + V(\mathbf{r})\mathbb{1}_4, \tag{1}$$

where H_{K} is the kinetic energy, H_{ε} describes the effects of strains, H_{Z} is the Zeeman Hamiltonian and $\mathbb{1}_4$ is the 4×4 identity matrix [41]. H_{K} and H_{ε} share the same generic form in the $J_z = \{+\frac{3}{2}, +\frac{1}{2}, -\frac{1}{2}, -\frac{3}{2}\}$ basis set:

$$H_{\mathrm{K}/\varepsilon} = \begin{pmatrix} P+Q & -S & R & 0 \\ -S^{\dagger} & P-Q & 0 & R \\ R^{\dagger} & 0 & P-Q & S \\ 0 & R^{\dagger} & S^{\dagger} & P+Q \end{pmatrix}, \tag{2}$$

where, for H_{K},

$$P_{\mathrm{K}} = \frac{1}{2m_0}\gamma_1(p_x^2 + p_y^2 + p_z^2), \tag{3a}$$

 © 2023 American Physical Society

$$Q_{\rm K} = \frac{1}{2m_0}\gamma_2(p_x^2 + p_y^2 - 2p_z^2), \tag{3b}$$

$$R_{\rm K} = \frac{1}{2m_0}\sqrt{3}[-\gamma_2(p_x^2 - p_y^2) + 2i\gamma_3\{p_x, p_y\}], \tag{3c}$$

$$S_{\rm K} = \frac{1}{2m_0}2\sqrt{3}\gamma_3\{p_x - ip_y, p_z\}, \tag{3d}$$

with $\{A, B\} = \frac{1}{2}(AB + BA)$, and, for H_ε,

$$P_\varepsilon = -a_v(\varepsilon_{xx} + \varepsilon_{yy} + \varepsilon_{zz}), \tag{4a}$$

$$Q_\varepsilon = -\frac{1}{2}b_v(\varepsilon_{xx} + \varepsilon_{yy} - 2\varepsilon_{zz}), \tag{4b}$$

$$R_\varepsilon = \frac{\sqrt{3}}{2}b_v(\varepsilon_{xx} - \varepsilon_{yy}) - id_v\varepsilon_{xy}, \tag{4c}$$

$$S_\varepsilon = -d_v(\varepsilon_{xz} - i\varepsilon_{yz}). \tag{4d}$$

Here $\mathbf{p}$ is the momentum, m_0 is the free electron mass, and $\gamma_1, \gamma_2, \gamma_3$ are the Luttinger parameters that characterize the hole masses. The $\varepsilon_{\alpha\beta}$ are the strains; a_v is the hydrostatic, b_v the uniaxial and d_v the shear deformation potential of the valence band. The form of Eq. (2), which couples different J_z's through the R and S terms, embodies the action of SOI in the valence band. The Zeeman Hamiltonian $H_{\rm Z} = 2\mu_B(\kappa\mathbf{B}\cdot\mathbf{J} + q\mathbf{B}\cdot\mathbf{J}^3)$ describes the action of the magnetic field on the Bloch functions, with $\mathbf{J}$ the spin $\frac{3}{2}$ operator, $\mathbf{J}^3 \equiv (J_x^3, J_y^3, J_z^3)$, μ_B the Bohr magneton, and κ, q the isotropic and cubic Zeeman parameters. The action of $\mathbf{B}$ on the envelopes of the hole is accounted for by the substitution $\mathbf{p} \to -i\hbar\nabla + e\mathbf{A}$ in $H_{\rm K}$, with $\mathbf{A} = \frac{1}{2}\mathbf{B}\times\mathbf{r}$ the magnetic vector potential.

At $\mathbf{B} = \mathbf{0}$, the hole states are twofold degenerate owing to time-reversal symmetry. Each Kramers doublet splits at finite magnetic field and can be characterized by an effective Hamiltonian $\mathcal{H} = \frac{1}{2}\mu_B\boldsymbol{\sigma}\cdot g\mathbf{B}$, where $\boldsymbol{\sigma}$ is the vector of Pauli matrices and g is the gyromagnetic matrix of the doublet [6,27]. We consider from now on a quantum dot strongly confined along $z = [001]$ (e.g., hosted in a quantum well with thickness $L_{\rm W}$), although the following discussion can be extended to arbitrary structures. In the absence of HH/LH mixing [$R = S = 0$ in Eq. (2)], the ground state is a pure $\{|+\frac{3}{2}\rangle, |-\frac{3}{2}\rangle\}$ doublet split by $H_{\rm Z}$, with diagonal g matrix ($g_{xx} = -g_{yy} = 3q$, $g_{zz} = 6\kappa + (27/2)q$). $R_{\rm K}$ and $S_{\rm K}$ actually admix LH components into the HH ground state, owing, in particular, to lateral confinement in the xy plane. The effects of this admixture on the g matrix can be captured by a Schrieffer-Wolff (SW) transformation [42]:

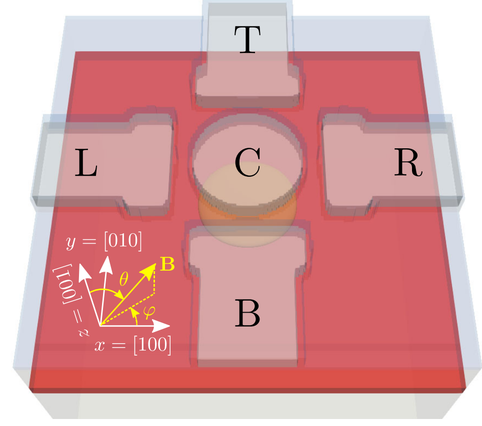

FIG. 1. The simulated device is made of 20 nm thick Al gates (gray) on a $Ge/Ge_{0.8}Si_{0.2}$ heterostructure with a $L_{\rm W} = 16$ nm thick Ge well (red) and a 50 nm thick upper GeSi barrier. The central C gate (diameter 100 nm) is separated from the L/R/T/B side gates by 20 nm. The gates are insulated from the substrate (and are surrounded on all facets) by 5 nm of Al_2O_3 (blue). The yellow shape is the isodensity surface that encloses 90% of the ground-state hole charge at bias $V_{\rm C} = -40$ mV with side gates grounded.

$$\delta\mathcal{H}_{hh'} \approx \sum_l \frac{1}{E_h - E_l}\langle h|H_{\rm c}|l\rangle\langle l|H'_{\rm c}|h'\rangle, \tag{5}$$

where h, h' run over the ground-state HH doublet with energy $E_{h'} = E_h$, l runs over LH states with energies E_l, and $H_{\rm c}, H'_{\rm c} \in \{R_{\rm K}, S_{\rm K}, H_{\rm Z}\}$. This yields [34,42]

$$g_{xx} \approx +3q + \frac{6}{m_0\Delta_{\rm LH}}(\lambda\langle p_x^2\rangle - \lambda'\langle p_y^2\rangle), \tag{6a}$$

$$g_{yy} \approx -3q - \frac{6}{m_0\Delta_{\rm LH}}(\lambda\langle p_y^2\rangle - \lambda'\langle p_x^2\rangle), \tag{6b}$$

$$g_{zz} \approx 6\kappa + \frac{27}{2}q - 2\gamma_h, \tag{6c}$$

where $\Delta_{\rm LH} = (2\pi^2\hbar^2\gamma_2/m_0L_{\rm W}^2)$ is the HH-LH band gap, $\lambda = \kappa\gamma_2 - 2\eta_h\gamma_3^2$, $\lambda' = \kappa\gamma_2 - 2\eta_h\gamma_2\gamma_3$, $\gamma_h \approx 3.56$ and $\eta_h \approx 0.20$ in unstrained Ge films [42–44]. The expectations values of p_x and p_y are calculated for the ground-state HH envelope of the quantum dot. The $\propto \kappa\gamma_2$ contributions to g_{xx} and g_{yy} result from the interplay between $H_{\rm Z}$ and $R_{\rm K}$, while the $\propto \eta_h$ terms result from the action of the magnetic vector potential in $R_{\rm K}$ and the interplay with $S_{\rm K}$. We have assumed here $\langle p_\alpha p_\beta\rangle = 0$ if $\alpha \neq \beta$ [42].

The strain terms R_ε and S_ε also mix HH and LH states and give rise to g-matrix corrections. Neglecting orbital excitation energies with respect to the HH/LH band gap ($E_l - E_h \approx \Delta_{\rm LH}$), and using $\sum_l\langle\mathbf{r}|l\rangle\langle l|\mathbf{r}'\rangle = \delta(\mathbf{r} - \mathbf{r}')$, we get from the interplay between H_ε and $H_{\rm Z}$:

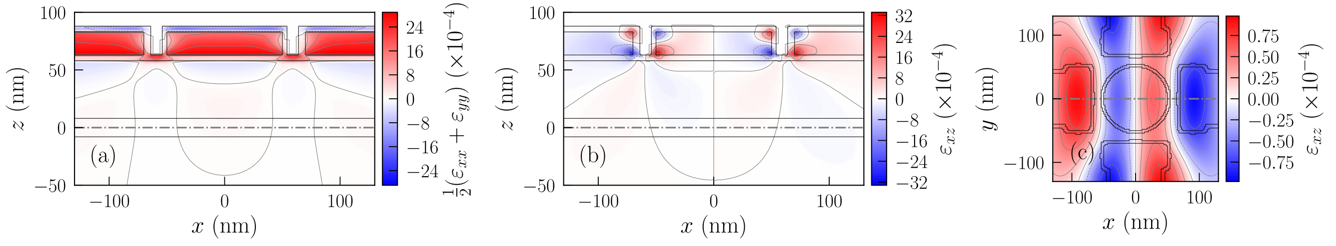

FIG. 2. Difference between inhomogeneous (with TC) and biaxial strains, in (a),(b) the xz plane at $y=0$, and (c) the xy plane at $z=0$. These planes are identified by dashed-dotted gray lines in the panels. The black lines delineate the materials in (a),(b) and the position of the gates (and Al_2O_3 around) at the surface of the heterostructure in (c). The strain ε_{yz} in the Ge well is obtained from panel (c) by a 90° rotation [46]. These maps are representative of the TC-induced strains in the device.

$$\delta g_{xx} = \delta g_{yy} = \frac{6b_v\kappa}{\Delta_{\rm LH}}(\langle\varepsilon_{yy}\rangle - \langle\varepsilon_{xx}\rangle), \tag{7a}$$

$$\delta g_{zy} = -\frac{4\sqrt{3}\kappa d_v}{\Delta_{\rm LH}}\langle\varepsilon_{yz}\rangle, \tag{7b}$$

$$\delta g_{zx} = -\frac{4\sqrt{3}\kappa d_v}{\Delta_{\rm LH}}\langle\varepsilon_{xz}\rangle, \tag{7c}$$

$$\delta g_{xy} = -\delta g_{yx} = \frac{4\sqrt{3}d_v\kappa}{\Delta_{\rm LH}}\langle\varepsilon_{xy}\rangle. \tag{7d}$$

We have dropped the smaller $\propto q$ terms. Under biaxial strain $\varepsilon_{xx}=\varepsilon_{yy}=\varepsilon_\parallel$, $\varepsilon_{zz}=\varepsilon_\perp$, $\Delta_{\rm LH}\approx(2\pi^2\hbar^2\gamma_2/m_0L_{\rm W}^2)+2b_v(\varepsilon_\parallel-\varepsilon_\perp)$ but the above corrections are zero. Shear strains may bring nonzero off-diagonal elements in the g matrix that rotate the principal magnetic axes as evidenced experimentally in Refs. [18,38].

Moreover, the interplay between H_ε and $H_{\rm K}$ gives rise to specific Rashba- and Dresselhaus-like SOIs. In particular, setting $H_{\rm c}=R_{\rm K}$, $H_{\rm c}'=S_\varepsilon$ (or vice versa) yields

$$\delta\mathcal{H}_{\rm so} = -\frac{\hbar}{m_\parallel}\left[\frac{1}{\ell_{\rm so}}p_x - i\frac{\hbar}{2}\left(\frac{\partial}{\partial x}\frac{1}{\ell_{\rm so}}\right)\right]\sigma_y, \tag{8}$$

with $m_\parallel$ the in-plane HH mass and $\ell_{\rm so}$ the spin-orbit length:

$$\frac{1}{\ell_{\rm so}} = \sqrt{3}\frac{m_\parallel d_v}{m_0\Delta_{\rm LH}}\left(\gamma_2\frac{\partial\varepsilon_{xz}}{\partial x} - \gamma_3\frac{\partial\varepsilon_{yz}}{\partial y}\right). \tag{9}$$

Note that $\ell_{\rm so}$ is generally dependent on position and signed [hence the $\propto(\partial/\partial x)(\ell_{\rm so}^{-1})$ correction for Hermiticity] [45]. It is remarkable that inhomogeneous strains promote linear-in-momentum (instead of cubic) SOI even in symmetric dots. The complete set of strain-induced SOIs is given in the Supplemental Material [46].

In general, g is dependent on the gate voltages, which gives rise to Rabi oscillations when driving the dot with a resonant ac signal [6,25,27]. The Rabi frequency reads

$$f_{\rm R} = \frac{\mu_B B V_{\rm ac}}{2hg^*}|g\mathbf{b}\times g'\mathbf{b}|, \tag{10}$$

where $\mathbf{b}$ is the unit vector along $\mathbf{B}$, $g^*=|g\mathbf{b}|$ is the effective g factor of the dot, $V_{\rm ac}$ is the amplitude of the drive and $g'=(\partial/\partial V)g$ is the derivative of g with respect to the driven gate voltage. The latter collects different contributions [27]: Kinetic Rashba SOI [28–30], also resulting from the interplay between $R_{\rm K}$ and $S_{\rm K}$ in Eq. (5), can give rise to nonzero off-diagonal elements in g' when the dot is shaken as a whole [6,42]; the deformations of the dot in an anharmonic confinement potential and/or an inhomogeneous ac field directly modulate $\langle p_x^2\rangle$ and $\langle p_y^2\rangle$, hence g_{xx}, g_{yy}, and g_{zz} (conventional g-TMR) [6,25,34]; the nonseparability of the confinement in the xy plane and along z can result in rotations of the principal axes of the g matrix and in nonzero g_{zx}' and g_{zy}' [34]. Finally, and this is the focus of this Letter, the motion and deformation of the dot in inhomogeneous strains can give rise to modulations of the $\delta g_{\alpha\beta}$'s [Eqs. (7)] as well as to strain-induced Rashba SOI [Eq. (9)].

Application and discussion.—As an illustration, we explore the contribution of these mechanisms to the Rabi oscillations of a hole spin qubit in a planar $Ge/Ge_{0.8}Si_{0.2}$ heterostructure [11,19–21]. We consider the device of Fig. 1, similar to Ref. [34]. The quantum dot is shaped by the central C gate with the side L/R/T/B gates grounded. Practically, the C and side gates may be on different metalization levels [21]; we keep, however, the structure as simple and symmetric as possible in order to best highlight the effects of strains. In the absence of the gate stack, the Ge well is biaxially strained by the $Ge_{0.8}Si_{0.2}$ buffer, with $\varepsilon_\parallel=-0.61\%$ and $\varepsilon_\perp=+0.45\%$. However, the Al gates and Al_2O_3 oxide imprint inhomogeneous strains resulting from fabrication and cool down. We assume here that the gate stack materials are nearly matched to the buffer at the temperature of their deposition ($T\approx300$ K for Al and $T\approx550$ K for Al_2O_3) and that inhomogeneous strains build up at $T\approx0$ K owing to the different thermal contraction (TC) coefficients (see Ref. [46] for details). This approach has been very successful in explaining the ESR line shapes of Si:Bi substrates with Al resonators on top

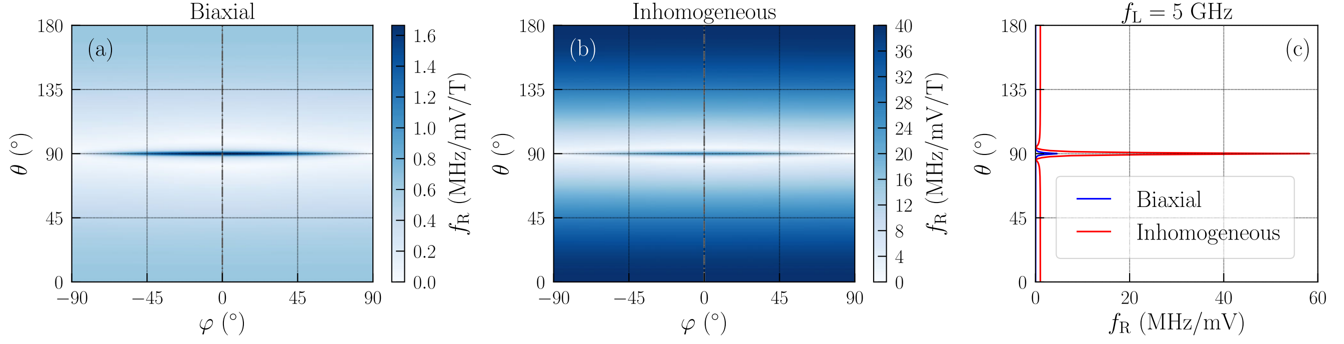

FIG. 3. (a),(b) Maps of Rabi frequency as a function of the orientation of the magnetic field, for opposite drives $\delta V_L = -\delta V_R = \frac{1}{2} V_{ac} \cos 2\pi f_L t$ on the L and R gates ($V_C = -40$ mV). Map (a) is for homogeneous biaxial strains, and map (b) is with inhomogeneous TC strains. The Rabi frequency, proportional to B and V_{ac}, is normalized to $B = 1$ T and $V_{ac} = 1$ mV. (c) Rabi frequency as a function of θ ($\varphi = 0$) at constant Larmor frequency $f_L = 5$ GHz, normalized to $V_{ac} = 1$ mV.

[37,60]. The strains are calculated with a finite-element approach [46].

The differences between inhomogeneous (with TC) and biaxial strains are plotted in Fig. 2 (see Ref. [46] for other strain components). The TC strains are mostly induced by the Al gates that contract much faster than the oxide and semiconductors. The effective lattice mismatch between the Al gates and $Ge_{0.8}Si_{0.2}$ buffer is indeed $\Delta a/a \approx -0.35\%$ at $T = 0$ K. The large $\varepsilon_p = \frac{1}{2}(\varepsilon_{xx} + \varepsilon_{yy}) \approx 0.27\%$ at the bottom interface of the C gate shows, however, that the contraction of Al is strongly hindered by the harder buffer and oxide. The strain modulations within the heterostructure are therefore small, with prominent shear components. They decrease with depth, reaching at most $\varepsilon_p - \varepsilon_\parallel \approx 0.007\%$ in the Ge well. We emphasize that the existence of such strains has been recently demonstrated experimentally in a similar layout [61].

The electrical potential of the gates is computed with a finite-volumes method and the eigenstates of the dots with a finite-difference discretization of Eq. (1). The Rabi frequencies are then calculated from the numerical g matrix and its derivative [27,46]. This g-matrix formalism is nonperturbative in the HH/LH mixings and includes, therefore, all orders beyond Eqs. (7) and (8). The maps of Rabi frequency as a function of the orientation of **B** are plotted in Fig. 3 for biaxial and inhomogeneous strains. The hole is driven by opposite ac modulations $\delta V_L = -\delta V_R = \frac{1}{2} V_{ac} \cos 2\pi f_L t$ on the L and R gates, where $f_L = g^* \mu_B B/h$ is the Larmor frequency (see Ref. [46] for drives with the L or C gate only). The maximal Rabi frequency (at constant f_L) is enhanced by a factor ≈13 by inhomogeneous CT strains. The anisotropy is nonetheless similar as in biaxial strains. Indeed, the first-order corrections $\delta g_{\alpha\beta}$ are all zero at $V_L = V_R = 0$ given the symmetries of the device. The g factors of the undriven dot are therefore almost the same in biaxial and in homogeneous strains. Moreover, only $g'_{xz} = \partial g_{xz}/\partial V_{LR}$ and $g'_{zx} = \partial g_{zx}/\partial V_{LR}$ (with $V_{LR} = V_L - V_R$) can be nonzero in both cases owing to the parity of the ac electric field [27,34,46]. Therefore, for **B** in the xz plane,

$$f_R(\theta) = \frac{\mu_B B V_{ac}}{2hg^*} |g'_{xz} g_\perp \cos^2\theta - g'_{zx} g_\parallel \sin^2\theta|, \quad (11)$$

and for **B** in the xy plane,

$$f_R(\varphi) = \frac{\mu_B B V_{ac}}{2h} |g'_{zx} \cos\varphi|, \quad (12)$$

where $g_\perp \equiv g_{zz} \approx 13.5$, $g_\parallel \equiv g_{xx} = -g_{yy} \approx 0.15$, and $g^* = \sqrt{g_\perp^2 \cos^2\theta + g_\parallel^2 \sin^2\theta}$ [34,62]. Thus g'_{xz} rules the out-of-plane, $\propto |b_z|$ background of Figs. 3(a) and 3(b), while g'_{zx} gives rise to the in-plane, $\propto |b_x|$ feature. The latter is particularly sharp (especially at constant f_L) owing to the very large ratio between $g_\perp$ and $g_\parallel$. The mechanisms responsible for the Rabi oscillations in biaxial strains have been discussed in Ref. [34]. The out-of-plane background ($g'_{xz} = 0.09$ V^{-1}) stems from cubic Rashba SOI, while the in-plane feature ($g'_{zx} = 0.24$ V^{-1}) is g-TMR resulting from the coupling between the motions along x/y and z in the nonseparable confinement potential of the holes.

These mechanisms are superseded in inhomogeneous strains by the effects of the shear strains ε_{xz} and ε_{yz} (the other $\varepsilon_{\alpha\beta}$ making only minor contributions). The in-plane feature now picks the modulations of Eq. (7c) when the dot moves in the ε_{xz} gradient. This is hence a g-TMR contribution, however leveraging the displacement $x'_d = \partial\langle x\rangle/\partial V_{LR}$ of the dot rather than its deformations [6,25]. Using the calculated $x'_d = 1.15$ nm/mV and the biaxial HH/LH band gap $\Delta_{LH} \approx 71$ meV, we estimate $\delta g'_{zx} \approx -4\sqrt{3}\kappa d_v x'_d \langle(\partial/\partial x)\varepsilon_{xz}\rangle/\Delta_{LH} \approx 3.84$ V^{-1} from Eq. (7c). This is actually more than one decade larger than $g'_{zx} = 0.24$ V^{-1} in biaxial strains, and in fair agreement with the numerical (non-perturbative) $g'_{zx} = 3.25$ V^{-1}, which shows that the SW transformation captures the main features of

the strain-induced SOI. The physics of the strain-induced Rashba SOI, Eq. (8), is more intricate. If $\ell_{\rm so}$ is homogeneous (constant $(\partial/\partial x)\varepsilon_{xz}$ and $(\partial/\partial y)\varepsilon_{yz}$), $\delta\mathcal{H}_{\rm so}$ essentially couples the spin to the velocity $v_x = -(V_{\rm ac}x'_{\rm d})2\pi f_{\rm L}\sin(2\pi f_{\rm L}t)$ of the driven hole, which results in a Rabi frequency $f_{\rm R} = V_{\rm ac}x'_{\rm d}f_{\rm L}/\ell_{\rm so}$ when $\mathbf{B}\perp\mathbf{y}$ [24]. In the g-matrix formalism, this translates into a small correction $-2g_{\parallel}x'_{\rm d}/\ell_{\rm so}$ to g'_{zx}, and into a sizable contribution $2g_{\perp}x'_{\rm d}/\ell_{\rm so}$ to g'_{xz} [46]. However, when the spin-orbit lengths are inhomogeneous, the orbital motion of the hole in the magnetic vector potential becomes dependent on the dot position through the substitution $\mathbf{p}\rightarrow -i\hbar\boldsymbol{\nabla} + e\mathbf{A}$ in $\delta\mathcal{H}_{\rm so}$, which makes an even larger contribution to g'_{xz}. From $g'_{xz} = 1.52\ \mathrm{V}^{-1}$ without magnetic vector potential in $H_{\rm K}$, we estimate an effective $\ell_{\rm so} = 2g_{\perp}x'_{\rm d}/g'_{xz} = 32\ \mu\mathrm{m}$, close to the expectation value of Eq. (9), $\ell_{\rm so} = 40\ \mu\mathrm{m}$; with the magnetic vector potential back on, $g'_{xz} = 5.70\ \mathrm{V}^{-1}$ actually increases by a factor 4 (and is larger than the cubic Rashba contribution $g'_{xz} = 0.09\ \mathrm{V}^{-1}$ by a factor 63). This large g'_{xz} can, however, hardly be harnessed efficiently because the magnetic field is much smaller along z than in plane at given $f_{\rm L}$ ($g_{\perp}\gg g_{\parallel}$). Rabi frequencies are practically larger for in-plane magnetic fields, and look more consistent with experimental data in inhomogeneous strains [20,21] ($f_{\rm R}$ in the 50 MHz range indeed imply unreasonably large peak-to-peak modulations $2V_{\rm ac}\approx 20$ mV in biaxial strains).

In the present device, the strain gradients are $(\partial/\partial x)\varepsilon_{xz} = (\partial/\partial y)\varepsilon_{yz}\approx 3\times 10^{-6}\ \mathrm{nm}^{-1}$ at the center of the dot. Residual shear strain gradients as small as $10^{-7}\ \mathrm{nm}^{-1}$ would, therefore, still enhance significantly the Rabi frequencies. We emphasize that the strains are primarily imposed by the same gates that shape the potential; they are therefore pervasive and commensurate with the dots, which strengthens their efficiency. Also, $f_{\rm R}$ is $\propto x'_{\rm d}\propto r_{\parallel}^4$ for both strain-induced g-TMR and Rashba SOI, with $r_{\parallel}$ the radius of the dot. This is an unusually strong scaling for g-TMR contributions such as $\delta g'_{zx}$ (Rashba SOI typically prevailing over purely kinetic g-TMR in long dots [42]). Strain-induced g-TMR shall, therefore, dominate over Rashba interactions whatever the size of the dot. Moreover, Fig. 2(b) suggests that the Rabi oscillations speed up considerably if the Ge well is brought closer to the Al gates where shear strains are maximal. Calculations for a 25 nm thick $\mathrm{Ge_{0.8}Si_{0.2}}$ barrier indeed show a 2.2× enhancement of the Rabi frequencies [46]. The prevalence of the above mechanisms can most easily be demonstrated experimentally by varying the nature or thickness of the metal gates, which has negligible impact on the electrostatics of a deeply buried well but modulates the strains in the heterostructure [46]. Finally, we would like to outline the role of strain-induced SOI on the dephasing time T_2^*. Although stronger SOI is expected to decrease T_2^*, we find that inhomogeneously strained devices actually exhibit better quality factors $Q_2^* = 2f_{\rm R}T_2^*$ over a wide range of magnetic-field orientations thanks to the strong enhancement of the Rabi frequency $f_{\rm R}$. Moreover, biaxially and inhomogeneously strained devices display the same "sweet spot" $\mathbf{B}\parallel\mathbf{x}$ that maximizes Q_2^* owing to symmetry and reciprocal sweetness relations between $f_{\rm R}$ and T_2^* [15]. Decoherence and relaxation are discussed in more detail in the Supplemental Material [46].

To conclude, we have unveiled the specific linear Rashba SOI and g-TMR mechanisms arising from the motion of holes in inhomogeneous strain fields. In planar heterostructures, these mechanisms are essentially ruled by the gradients of shear strains ε_{xz} and ε_{yz}. In Ge/GeSi spin qubits, they can make a prevalent contribution to the Rabi frequency even for the small shear strain gradients achieved by differential thermal contraction upon cool down. These mechanisms highlight the role of strains in spin-orbit physics and open the way for strain engineering in hole spin devices for quantum information [19], hybrid semiconductor-superconductor and topological physics [63,64], and spintronics [65,66].

We thank R. Maurand for fruitful discussions and comments on the manuscript. This work was supported by the French National Research Agency (ANR) through the MAQSi project and the "France 2030" program (PEPR PRESQUILE—ANR-22-PETQ-0002).

*yniquet@cea.fr

[1] G. Burkard, T. D. Ladd, J. M. Nichol, A. Pan, and J. R. Petta, Semiconductor spin qubits, Rev. Mod. Phys. **95**, 025003 (2023).
[2] R. Winkler, *Spin-Orbit Coupling in Two-Dimensional Electron and Hole Systems* (Springer, Berlin, 2003).
[3] C. Kloeffel, M. Trif, and D. Loss, Strong spin-orbit interaction and helical hole states in Ge/Si nanowires, Phys. Rev. B **84**, 195314 (2011).
[4] C. Kloeffel, M. J. Rančić, and D. Loss, Direct Rashba spin-orbit interaction in Si and Ge nanowires with different growth directions, Phys. Rev. B **97**, 235422 (2018).
[5] R. Maurand, X. Jehl, D. Kotekar-Patil, A. Corna, H. Bohuslavskyi, R. Laviéville, L. Hutin, S. Barraud, M. Vinet, M. Sanquer, and S. de Franceschi, A CMOS silicon spin qubit, Nat. Commun. **7**, 13575 (2016).
[6] A. Crippa, R. Maurand, L. Bourdet, D. Kotekar-Patil, A. Amisse, X. Jehl, M. Sanquer, R. Laviéville, H. Bohuslavskyi, L. Hutin, S. Barraud, M. Vinet, Y.-M. Niquet, and S. De Franceschi, Electrical Spin Driving by g-Matrix Modulation in Spin-Orbit Qubits, Phys. Rev. Lett. **120**, 137702 (2018).
[7] H. Watzinger, J. Kukučka, L. Vukušić, F. Gao, T. Wang, F. Schäffler, J.-J. Zhang, and G. Katsaros, A germanium hole spin qubit, Nat. Commun. **9**, 3902 (2018).
[8] L. C. Camenzind, S. Geyer, A. Fuhrer, R. J. Warburton, D. M. Zumbühl, and A. V. Kuhlmann, A hole spin qubit in a fin field-effect transistor above 4 kelvin, Nat. Electron. **5**, 178 (2022).

[9] F. N. M. Froning, L. C. Camenzind, O. A. H. van der Molen, A. Li, E. P. A. M. Bakkers, D. M. Zumbühl, and F. R. Braakman, Ultrafast hole spin qubit with gate-tunable spin-orbit switch functionality, Nat. Nanotechnol. **16**, 308 (2021).

[10] K. Wang, G. Xu, F. Gao, H. Liu, R.-L. Ma, X. Zhang, Z. Wang, G. Cao, T. Wang, J.-J. Zhang, D. Culcer, X. Hu, H.-W. Jiang, H.-O. Li, G.-C. Guo, and G.-P. Guo, Ultrafast coherent control of a hole spin qubit in a germanium quantum dot, Nat. Commun. **13**, 206 (2022).

[11] N. W. Hendrickx, W. I. L. Lawrie, L. Petit, A. Sammak, G. Scappucci, and M. Veldhorst, A single-hole spin qubit, Nat. Commun. **11**, 3478 (2020).

[12] C. Kloeffel, M. Trif, P. Stano, and D. Loss, Circuit QED with hole-spin qubits in Ge/Si nanowire quantum dots, Phys. Rev. B **88**, 241405(R) (2013).

[13] S. Bosco, P. Scarlino, J. Klinovaja, and D. Loss, Fully Tunable Longitudinal Spin-Photon Interactions in Si and Ge Quantum Dots, Phys. Rev. Lett. **129**, 066801 (2022).

[14] C. X. Yu, S. Zihlmann, J. C. Abadillo-Uriel, V. P. Michal, N. Rambal, H. Niebojewski, T. Bedecarrats, M. Vinet, É. Dumur, M. Filippone *et al.*, Strong coupling between a photon and a hole spin in silicon, Nat. Nanotechnol. 18, 741 (2023).

[15] V. P. Michal, J. C. Abadillo-Uriel, S. Zihlmann, R. Maurand, Y.-M. Niquet, and M. Filippone, Tunable hole spin-photon interaction based on *g*-matrix modulation, Phys. Rev. B **107**, L041303 (2023).

[16] Z. Wang, E. Marcellina, A. R. Hamilton, J. H. Cullen, S. Rogge, J. Salfi, and D. Culcer, Optimal operation points for ultrafast, highly coherent Ge hole spin-orbit qubits, npj Quantum Inf. **7**, 54 (2021).

[17] S. Bosco, B. Hetényi, and D. Loss, Hole spin qubits in Si FinFETs with fully tunable spin-orbit coupling and sweet spots for charge noise, PRX Quantum **2**, 010348 (2021).

[18] N. Piot, B. Brun, V. Schmitt, S. Zihlmann, V. P. Michal, A. Apra, J. C. Abadillo-Uriel, X. Jehl, B. Bertrand, H. Niebojewski, L. Hutin, M. Vinet, M. Urdampilleta, T. Meunier, Y.-M. Niquet, R. Maurand, and S. De Franceschi, A single hole spin with enhanced coherence in natural silicon, Nat. Nanotechnol. **17**, 1072 (2022).

[19] G. Scappucci, C. Kloeffel, F. A. Zwanenburg, D. Loss, M. Myronov, J.-J. Zhang, S. De Franceschi, G. Katsaros, and M. Veldhorst, The germanium quantum information route, Nat. Rev. Mater. **6**, 926 (2021).

[20] N. W. Hendrickx, D. P. Franke, A. Sammak, G. Scappucci, and M. Veldhorst, Fast two-qubit logic with holes in germanium, Nature (London) **577**, 487 (2020).

[21] N. W. Hendrickx, I. L. Lawrie William, M. Russ, F. van Riggelen, S. L. de Snoo, R. N. Schouten, A. Sammak, G. Scappucci, and M. Veldhorst, A four-qubit germanium quantum processor, Nature (London) **591**, 580 (2021).

[22] F. Borsoi, N. W. Hendrickx, V. John, S. Motz, F. van Riggelen, A. Sammak, S. L. de Snoo, G. Scappucci, and M. Veldhorst, Shared control of a 16 semiconductor quantum dot crossbar array, arXiv:2209.06609.

[23] E. I. Rashba and A. L. Efros, Orbital Mechanisms of Electron-Spin Manipulation by an Electric Field, Phys. Rev. Lett. **91**, 126405 (2003).

[24] V. N. Golovach, M. Borhani, and D. Loss, Electric-dipole-induced spin resonance in quantum dots, Phys. Rev. B **74**, 165319 (2006).

[25] Y. Kato, R. C. Myers, D. C. Driscoll, A. C. Gossard, J. Levy, and D. D. Awschalom, Gigahertz electron spin manipulation using voltage-controlled *g*-tensor modulation, Science **299**, 1201 (2003).

[26] N. Ares, G. Katsaros, V. N. Golovach, J. J. Zhang, A. Prager, L. I. Glazman, O. G. Schmidt, and S. De Franceschi, SiGe quantum dots for fast hole spin Rabi oscillations, Appl. Phys. Lett. **103**, 263113 (2013).

[27] B. Venitucci, L. Bourdet, D. Pouzada, and Y.-M. Niquet, Electrical manipulation of semiconductor spin qubits within the *g*-matrix formalism, Phys. Rev. B **98**, 155319 (2018).

[28] E. Marcellina, A. R. Hamilton, R. Winkler, and D. Culcer, Spin-orbit interactions in inversion-asymmetric two-dimensional hole systems: A variational analysis, Phys. Rev. B **95**, 075305 (2017).

[29] L. A. Terrazos, E. Marcellina, Z. Wang, S. N. Coppersmith, M. Friesen, A. R. Hamilton, X. Hu, B. Koiller, A. L. Saraiva, D. Culcer, and R. B. Capaz, Theory of hole-spin qubits in strained germanium quantum dots, Phys. Rev. B **103**, 125201 (2021).

[30] S. Bosco, M. Benito, C. Adelsberger, and D. Loss, Squeezed hole spin qubits in Ge quantum dots with ultrafast gates at low power, Phys. Rev. B **104**, 115425 (2021).

[31] Y. Liu, J.-X. Xiong, Z. Wang, W.-L. Ma, S. Guan, J.-W. Luo, and S.-S. Li, Emergent linear Rashba spin-orbit coupling offers fast manipulation of hole-spin qubits in germanium, Phys. Rev. B **105**, 075313 (2022).

[32] A. Ciocoiu, M. Khalifa, and J. Salfi, Towards computer-assisted design of hole spin qubits in quantum dot devices, arXiv:2209.12026.

[33] S. Bosco and D. Loss, Hole Spin Qubits in Thin Curved Quantum Wells, Phys. Rev. Appl. **18**, 044038 (2022).

[34] B. Martinez, J. C. Abadillo-Uriel, E. A. Rodríguez-Mena, and Y.-M. Niquet, Hole spin manipulation in inhomogeneous and nonseparable electric fields, Phys. Rev. B **106**, 235426 (2022).

[35] T. Thorbeck and N. M. Zimmerman, Formation of strain-induced quantum dots in gated semiconductor nanostructures, AIP Adv. **5**, 087107 (2015).

[36] J. Mansir, P. Conti, Z. Zeng, J. J. Pla, P. Bertet, M. W. Swift, C. G. Van de Walle, M. L. W. Thewalt, B. Sklenard, Y. M. Niquet, and J. J. L. Morton, Linear Hyperfine Tuning of Donor Spins in Silicon using Hydrostatic Strain, Phys. Rev. Lett. **120**, 167701 (2018).

[37] J. J. Pla, A. Bienfait, G. Pica, J. Mansir, F. A. Mohiyaddin, Z. Zeng, Y.-M. Niquet, A. Morello, T. Schenkel, J. J. L. Morton, and P. Bertet, Strain-Induced Spin-Resonance Shifts in Silicon Devices, Phys. Rev. Appl. **9**, 044014 (2018).

[38] S. D. Liles, F. Martins, D. S. Miserev, A. A. Kiselev, I. D. Thorvaldson, M. J. Rendell, I. K. Jin, F. E. Hudson, M. Veldhorst, K. M. Itoh, O. P. Sushkov, T. D. Ladd, A. S. Dzurak, and A. R. Hamilton, Electrical control of the *g* tensor of the first hole in a silicon MOS quantum dot, Phys. Rev. B **104**, 235303 (2021).

[39] J. M. Luttinger, Quantum theory of cyclotron resonance in semiconductors: General theory, Phys. Rev. **102**, 1030 (1956).

[40] L. C. Lew Yan Voon and M. Willatzen, *The k p Method* (Springer, Berlin, 2009).

[41] We assume here holes with positive (electron-like) dispersion.

[42] V. P. Michal, B. Venitucci, and Y.-M. Niquet, Longitudinal and transverse electric field manipulation of hole spin-orbit qubits in one-dimensional channels, Phys. Rev. B **103**, 045305 (2021).

[43] N. Ares, V. N. Golovach, G. Katsaros, M. Stoffel, F. Fournel, L. I. Glazman, O. G. Schmidt, and S. De Franceschi, Nature of Tunable Hole g Factors in Quantum Dots, Phys. Rev. Lett. **110**, 046602 (2013).

[44] In biaxial strains $\varepsilon_{\parallel} = -0.61\%$ and $\varepsilon_{\perp} = +0.45\%$, $\gamma_h \approx 2.62$ and $\eta_h \approx 0.41$ for $L_W = 16$ nm [34,42].

[45] F. Dolcini and F. Rossi, Magnetic field effects on a nanowire with inhomogeneous Rashba spin-orbit coupling: Spin properties at equilibrium, Phys. Rev. B **98**, 045436 (2018).

[46] See Supplemental Material at http://link.aps.org/supplemental/10.1103/PhysRevLett.131.097002 with the material parameters, the complete set of strains, the Rabi frequencies driven with the L or C gate only, the dependences on the top GeSi barrier, gate and oxide thicknesses, the full set of strain-induced SOIs, and a discussion about coherence and about g matrices; which includes Refs. [47–59].

[47] R. R. Reeber and K. Wang, Thermal expansion and lattice parameters of group IV semiconductors, Mater. Chem. Phys. **46**, 259 (1996).

[48] J. P. Dismukes, L. Ekstrom, and R. J. Paff, Lattice parameter and density in germanium-silicon alloys, J. Phys. Chem. **68**, 3021 (1964).

[49] J. J. Hall, Electronic effects in the elastic constants of n-type silicon, Phys. Rev. **161**, 756 (1967).

[50] M. E. Fine, Elastic constants of germanium between 1.7° and 80 °K, J. Appl. Phys. **26**, 862 (1955).

[51] J. Vallin, M. Mongy, K. Salama, and O. Beckman, Elastic constants of aluminum, J. Appl. Phys. **35**, 1825 (1964).

[52] M. K. Tripp, C. Stampfer, D. C. Miller, T. Helbling, C. F. Herrmann, C. Hierold, K. Gall, S. M. George, and V. M. Bright, The mechanical properties of atomic layer deposited alumina for use in micro- and nano-electromechanical systems, Sens. Actuators A **130**, 419 (2006).

[53] O. M. Ylivaara, X. Liu, L. Kilpi, J. Lyytinen, D. Schneider, M. Laitinen, J. Julin, S. Ali, S. Sintonen, M. Berdova, E. Haimi, T. Sajavaara, H. Ronkainen, H. Lipsanen, J. Koskinen, S.-P. Hannula, and R. L. Puurunen, Aluminum oxide from trimethylaluminum and water by atomic layer deposition: The temperature dependence of residual stress, elastic modulus, hardness and adhesion, Thin Solid Films **552**, 124 (2014).

[54] A. Sammak, D. Sabbagh, N. W. Hendrickx, M. Lodari, B. Paquelet Wuetz, A. Tosato, L. Yeoh, M. Bollani, M. Virgilio, M. A. Schubert, P. Zaumseil, G. Capellini, M. Veldhorst, and G. Scappucci, Shallow and undoped germanium quantum wells: A playground for spin and hybrid quantum technology, Adv. Funct. Mater. **29**, 1807613 (2019).

[55] F. C. Nix and D. MacNair, The thermal expansion of pure metals: Copper, gold, aluminum, nickel, and iron, Phys. Rev. **60**, 597 (1941).

[56] D. C. Miller, R. R. Foster, S.-H. Jen, J. A. Bertrand, S. J. Cunningham, A. S. Morris, Y.-C. Lee, S. M. George, and M. L. Dunn, Thermo-mechanical properties of alumina films created using the atomic layer deposition technique, Sens. Actuators A **164**, 58 (2010).

[57] M. V. Fischetti and S. E. Laux, Band structure, deformation potentials, and carrier mobility in strained Si, Ge, and SiGe alloys, J. Appl. Phys. **80**, 2234 (1996).

[58] J.-T. Hung, E. Marcellina, B. Wang, A. R. Hamilton, and D. Culcer, Spin blockade in hole quantum dots: Tuning exchange electrically and probing zeeman interactions, Phys. Rev. B **95**, 195316 (2017).

[59] J. Li, B. Venitucci, and Y.-M. Niquet, Hole-phonon interactions in quantum dots: Effects of phonon confinement and encapsulation materials on spin-orbit qubits, Phys. Rev. B **102**, 075415 (2020).

[60] V. Ranjan, B. Albanese, E. Albertinale, E. Billaud, D. Flanigan, J. J. Pla, T. Schenkel, D. Vion, D. Esteve, E. Flurin, J. J. L. Morton, Y. M. Niquet, and P. Bertet, Spatially Resolved Decoherence of Donor Spins in Silicon Strained by a Metallic Electrode, Phys. Rev. X **11**, 031036 (2021).

[61] C. Corley-Wiciak, C. Richter, M. H. Zoellner, I. Zaitsev, C. L. Manganelli, E. Zatterin, T. U. Schülli, A. A. Corley-Wiciak, J. Katzer, F. Reichmann, W. M. Klesse, N. W. Hendrickx, A. Sammak, M. Veldhorst, G. Scappucci, M. Virgilio, and G. Capellini, Nanoscale mapping of the 3D strain tensor in a germanium quantum well hosting a functional spin qubit device, ACS Appl. Mater. Interfaces **15**, 3119 (2023).

[62] C.-A. Wang, G. Scappucci, M. Veldhorst, and M. Russ, Modelling of planar germanium hole qubits in electric and magnetic fields, arXiv:2208.04795.

[63] F. Maier, J. Klinovaja, and D. Loss, Majorana fermions in Ge/Si hole nanowires, Phys. Rev. B **90**, 195421 (2014).

[64] N. W. Hendrickx, D. P. Franke, A. Sammak, M. Kouwenhoven, D. Sabbagh, L. Yeoh, R. Li, M. L. V. Tagliaferri, M. Virgilio, G. Capellini, G. Scappucci, and M. Veldhorst, Gate-controlled quantum dots and superconductivity in planar germanium, Nat. Commun. **9**, 2835 (2018).

[65] A. Hirohata, K. Yamada, Y. Nakatani, I.-L. Prejbeanu, B. Diény, P. Pirro, and B. Hillebrands, Review on spintronics: Principles and device applications, J. Magn. Magn. Mater. **509**, 166711 (2020).

[66] Y. B. Lyanda-Geller, Spin-related phenomena in spin 3/2 charge carrier holes systems, Solid State Commun. **352**, 114815 (2022).